Indian Journal of Chemical Technology
Vol. 33, March 2026, pp. 207-216
DOI: 10.56042/ijct.v33i2.22641

Thermodynamic optimization of pulsatile Cu–GO/water hybrid nanofluid flow in a magnetized porous cavity

N. Vinodhini*

Department of Mathematics, Saveetha Engineering College, Chennai-602105, India

*E-mail: vinodhini9208@gmail.com

Received 11 August 2025; accepted 13 February 2026

The enhancement of thermal performance with minimal thermodynamic irreversibility is a key requirement in the design of modern energy and thermal management systems, particularly those involving magnetized porous enclosures. The present study aims to numerically investigate entropy generation and thermodynamic optimization in a forced convection flow of a Cu–GO/water hybrid nanofluid confined within a square porous cavity subjected to a transverse magnetic field. The hybrid nanofluid behaviour is modeled using the Tiwari–Das formulation, while the porous medium is characterized by the Darcy–Brinkman–Forchheimer model. The cavity consists of stationary horizontal walls with centrally heated sections maintained at a constant high temperature, whereas the vertical walls are kept cold. The governing equations are solved numerically to analyze the effects of the Hartmann number, Darcy number, and nanoparticle volume fraction on heat transfer characteristics and entropy generation. The results reveal that the inclusion of graphene oxide nanoparticles significantly enhances heat transfer performance while suppressing entropy generation under appropriate magnetic field strengths and porous resistance conditions. The study concludes that Cu–GO hybrid nanofluids provide an effective thermodynamic optimization strategy for magnetohydrodynamic convection in porous cavity-based thermal systems.

Keywords: Copper nanoparticles, Finite difference, Heat sink/source, Graphene oxide, MHD convection

Introduction

The pursuit of efficient thermal management has become pivotal across various engineering applications, including microelectronics cooling, energy storage, and biomedical devices. Traditional heat transfer fluids often fail to meet the increasing thermal demands of modern technologies, which has led to the development of nanofluid and, more recently, hybrid nanofluids. Among these, the Cu–GO/water hybrid nanofluid offers a remarkable enhancement in thermal conductivity, synergizing the superior heat transport of copper with the high surface area and stability of graphene oxide. However, improvements in heat transfer must be balanced against thermodynamic losses, making entropy generation analysis critical in optimizing the energy efficiency of such systems. Porous cavities are widely employed in thermal engineering applications due to their ability to enhance heat transfer and regulate fluid flow. Accurate modeling of flow through porous media requires robust theoretical frameworks such as the Darcy–Brinkman–Forchheimer (DBF) model, which accounts for non-Darcy effects, including permeability resistance and inertial drag. The situation becomes more intricate when the influence of a transverse magnetic field, where Lorentz forces modulate the fluid motion, is relevant in magnetohydrodynamic (MHD) devices, electromagnetic cooling, and biomedical targeting systems. In practical thermal systems, heating is often localized rather than uniformly distributed. Motivated by this observation, the present study considers a dual localized heating configuration in which only the central portions of the horizontal walls are heated**,** while the vertical walls are maintained at a cold temperature**.** This configuration realistically represents applications such as localized electronic chip cooling and targeted hyperthermia treatments. Furthermore, pulsatile flow is incorporated to capture unsteady flow behaviour commonly encountered in physiological systems and oscillatory thermal processes**.** Despite its practical importance, the combined influence of pulsatile flow, hybrid nanofluid transport, magnetohydrodynamics, and non-Darcy porous resistance under localized heating conditions remains largely unexplored**.**

In this work, the Tiwari–Das model is employed to describe the hybrid nanofluid properties, while the

Darcy–Brinkman–Forchheimer model is used to represent the porous medium. A numerical investigation is carried out to analyze entropy generation and thermodynamic performance in pulsatile Cu–GO/water hybrid nanofluid flow within a square porous cavity subjected to a transverse magnetic field. The effects of key controlling parameters, including the Hartmann number, Darcy number, and nanoparticle volume fraction, are examined in terms of flow structure, temperature distribution, Nusselt number variation, and Bejan number behavior. The results demonstrate that appropriate combinations of magnetic field strength, porous resistance, and nanoparticle loading can significantly enhance heat transfer while minimizing entropy generation. By integrating hybrid nanofluid technology, magnetic field modulation, pulsatile flow dynamics, and localized thermal control, this study contributes to the development of high-efficiency thermal systems operating under complex physical constraints**.**

The interplay of nanofluid dynamics, magnetic field effects, and internal heat sources/sinks in confined geometries has garnered extensive attention due to its relevance in thermal management systems, energy storage devices, and biomedical applications. Yang *et al*.[1] investigated both experimental and numerical research to evaluate the transient thermal behaviour of a phase-change material (PCM)-based heat sink employing a rectangular cavity plate-fin structure. Their findings demonstrated enhanced thermal regulation through intermittent heating cycles. In a related study, Alsabery *et al.*[2] examined the influence of localized heat sources/sinks on natural convection within a square enclosure containing a central solid cylinder, where a nanoparticle-laden base fluid (nanofluid) was used to augment thermal performance. Armaghani *et al*.[3] studied mixed convective flow of an Al_2O_3–Cu/water hybrid nanofluid within an L-shaped enclosure subjected to MHD forces and localized thermal sources. Their numerical findings underscored the sensitivity of flow structure and heat transfer rate to magnetic field intensity and heat source positioning. Waqas *et al*.[4] analyzed entropy generation and hydrothermal behaviour of Cu–water nanofluid in a sinusoidal cavity, demonstrating that both wall waviness and nanoparticle concentration significantly affect energy dissipation and fluid motion. Asmadi *et al*.[5] numerically analyzed the behaviour of a Cu–Al_2O_3/water hybrid nanofluid in a tilted U-shaped cavity, employing vorticity analysis to assess the fluid's internal rotational characteristics, which are critical for the heat transfer enhancement. Rajarathinam *et al*.[6] studied MHD-assisted Cu–water nanofluid in a tilted porous cavity containing an isothermal solid block. Their results highlighted the combined effect of magnetic field strength and inclination flow stability and thermal transport. Rashad *et al*.[7] performed a detailed entropy generation investigation in an oblique porous square regime loaded with nanofluid under MHD natural convection. They systematically assessed how the position and magnitude of heat sources and sinks modulate thermodynamic irreversibility. Moayedi et al.[8] evaluated the thermal performance of Cu–water nanofluid in a vented cavity containing dual rotating cylinders. Their study incorporated various port configurations to analyze the impact of fluid entry and exit locations on convective enhancement. Emami *et al*.[9] examined the impact of cavity inclination and thermal boundary constraints on natural convection in Cu–water nanofluids within porous square enclosures. Their findings emphasized that geometric orientation and wall heating configurations play a pivotal role in determining thermal stratification and circulation patterns. Ebrahimi and Dadvand[10] numerically modeled the melting characteristics of nano-enhanced phase change materials (NePCMs) within a square cavity featuring two heat source–sink pairs. The study provided insight into phase front evolution under localized heating. Rashad *et al*.[11] employed an MHD-based numerical model to study nanofluid-saturated lid-driven square cavity. Incorporating localized heating and velocity slip boundary conditions, the study revealed complex flow-field modifications driven by Lorentz forces.Faraz *et al*.[12] considered natural convection in a Cu–water nanofluid-filled square cavity embedded in a hexagonal enclosure under non-uniform thermal boundary conditions. Their results underscored the role of geometrical constraints in modifying the thermal plume structure. Hidki *et al*.[13] examined heat transfer characteristics of a Cu–Al_2O_3/water hybrid nanofluid in a cavity containing two constant heat-flux bodies. Their simulations revealed a significant enhancement in convective efficiency attributable to nanoparticle synergy. Nanofluids have gained considerable attention for their potential to enhance heat transfer performance. Natural convection in square cavities

under magnetic field effects has been widely studied. Vinodhini and Prasad[14] numerically investigated natural convection of a micropolar fluid using the finite volume method. Rupa *et al.*[15] conducted a sensitivity analysis of micropolar hybrid nanofluid flow using response surface methodology, demonstrating the significant influence of governing parameters on optimized heat transfer performance. Zahoor *et al.*[16] numerically investigated thermal convection of a radiative hybrid nanofluid in unsteady Darcy–Forchheimer flow over a slipping spinning porous disk, highlighting the combined effects of porous resistance and thermal radiation on heat transfer behavior. Reddy *et al.*[17] implemented the homotopy analysis method to examine entropy-optimized two-phase nanofluid flow in a bioconvective non-Newtonian model with thermal radiation, emphasizing thermodynamic irreversibility minimization. Prakash *et al.*[18] reported improved natural convection heat transfer characteristics with the use of nanofluids.

Finally, Mansour *et al.*[19] examined MHD natural convection in a porous square cavity filled with Al_2O_3–Cu/water hybrid nanofluid, with emphasis on the configuration of internal heat sources and sinks and their role in thermodynamic optimization. A distinctive feature of the present study is the incorporation of dual localized heating**,** in which only the central portions of the horizontal walls are heated, while the vertical walls are kept cold. In addition, pulsatile convection is considered, representing unsteady flow behaviour commonly encountered in physiological and industrial systems. Despite its relevance, the combined effects of pulsatile hybrid nanofluid flow, MHD, and non-Darcy porous resistance under localized heating conditions have not been adequately addressed in the existing literature**.**

Mathematical Model

This study explores unsteady, laminar mixed convection of an electrically responsive hybrid nanofluid within a two-dimensional square cavity (L = H), subjected to a transverse magnetic field. The vertical walls are kept isothermally cold (T_c), while the central regions of horizontal walls are heated to a constant temperature (T_h), with the remaining horizontal sections thermally insulated. The working fluid is a dilute suspension of graphene oxide (GO) and copper (Cu) nanoparticles in water, assumed to exhibit local thermal equilibrium. Internal heat generation is considered, while Hall current and magnetic induction effects are neglected. The configuration, boundary conditions, and thermal zones are illustrated in Fig. 1. Table 1 enumerates the thermophysical properties of the nanofluid.

$$\frac{\partial u}{\partial x}+\frac{\partial v}{\partial y}=0 \qquad \ldots (1)$$

$$\frac{\partial u}{\partial t^*}+u\frac{\partial u}{\partial x}+v\frac{\partial u}{\partial y}=-\frac{1}{\rho_{hnf}}\frac{\partial p}{\partial x}+\frac{\mu_{hnf}}{\rho_{hnf}}\left[\frac{\partial^2 u}{\partial x^2}+\frac{\partial^2 u}{\partial y^2}\right] \qquad \ldots (2)$$

$$\frac{\partial v}{\partial t^*}+u\frac{\partial v}{\partial x}+v\frac{\partial v}{\partial y}=-\frac{1}{\rho_{hnf}}\frac{\partial p}{\partial y}+\frac{\mu_{hnf}}{\rho_{hnf}}\left[\frac{\partial^2 v}{\partial x^2}+\frac{\partial^2 v}{\partial y^2}\right]-\frac{\sigma_{hnf}B_0^2}{\rho_{hnf}}v+\frac{(\rho\beta)_{hnf}}{\rho_{hnf}}g(T-T_c) \qquad \ldots (3)$$

$$\frac{\partial T}{\partial t^*}+u\frac{\partial T}{\partial x}+v\frac{\partial T}{\partial y}=\alpha_{hnf}\left[\frac{\partial^2 T}{\partial x^2}+\frac{\partial^2 T}{\partial y^2}\right]+\frac{Q_0}{(\rho C_p)_{hnf}}(T-T_c) \qquad \ldots (4)$$

Boundary Framework

$t^* > 0,\quad x = 0, 0 \le y \le L,\quad u = v = 0,\quad \frac{\partial T}{\partial x} = 0$

$t^* > 0,\quad x = L, 0 \le y \le L,\quad u = v = 0,\quad \frac{\partial T}{\partial x} = 0$

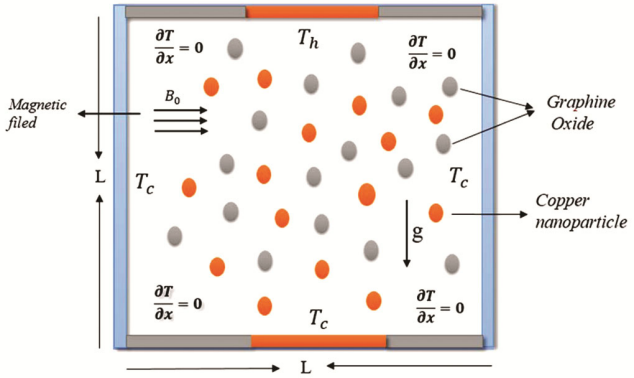

Fig. 1 — Schematic diagram of the model

Table 1 — Thermophysical properties of Cu, GO, and H_2O[20-22]

Property	Cu	Graphene Oxide (GO)	H_2O
ρ (kgm^{-3})	8,933	1800	997.1
$C_p(Jkg^{-1}K^{-1}$	385	717	4179
k (W$m^{-1}k^{-1}$)	401	5000	0.613
$\beta(k^{-1})$	1.67×10^{-5}	2.84×10^{-4}	21×10^{-5}
$\sigma(\Omega^{-1}m^{-1})$	5.96×10^{7}	6.30×10^{7}	0.05
μ	-	-	8.9×10^{-4}
Pr	-	-	6.2

$t^* > 0,\ y = 0, 0 \le x \le L,\ u = v = 0,\ \frac{\partial T}{\partial y} = 0$ for $0 \le x \le \frac{L}{4}$
$T = T_c$ for $\frac{L}{4} \le x \le \frac{3L}{4}$,
$\frac{\partial T}{\partial y} = 0$ for $\frac{3L}{4} \le x \le L$

$t^* > 0,\ y = L, 0 \le x \le L,\ u = v = 0,\ \frac{\partial T}{\partial y} = 0$ for $0 \le x \le \frac{L}{4}$
$T = T_h$ for $\frac{L}{4} \le x \le \frac{3L}{4}$,
$\frac{\partial T}{\partial y} = 0$ for $\frac{3L}{4} \le x \le L$

Thermophysical properties of hybrid nanofluids

Heat capacitance:

$$(\rho C_p)_{hnf} = (1-\varphi)(\rho C_p)_{bf} + \varphi_{GO}(\rho C_p)_{GO} + \varphi_{cu}(\rho C_p)_{cu} \quad \ldots (5)$$

Density:

$$\rho_{hnf} = (1-\varphi)\rho_{bf} + \varphi_{GO}\rho_{GO} + \varphi_{cu}\rho_{cu} \quad \ldots (6)$$

Thermal expansion coefficient:

$$(\rho\beta)_{hnf} = (1-\varphi)(\rho\beta)_{bf} + \varphi_{GO}(\rho\beta)_{GO} + \varphi_{cu}(\rho\beta)_{cu} \quad \ldots (7)$$

Electrical conductivity (Maxwell model):

$$\frac{\sigma_{hnf}}{\sigma_{bf}} = 1 + \frac{3(A-B)}{(A+2)-(A-B)} \quad \ldots (8)$$

Where $A = \frac{(\varphi_{GO}\sigma_{GO} + \varphi_{Ag}\sigma_{cu})}{\sigma_{bf}}$; $B = (\varphi_{GO} + \varphi_{cu})$

Thermal diffusivity and dynamic viscosity (Brinkman model):

$$\alpha_{hnf} = \frac{k_{hnf}}{(\rho C_p)_{hnf}} \text{and } \mu_{hnf} = \frac{\mu_{bf}}{(1-(\varphi_{GO}+\varphi_{cu}))^{2.5}} \quad \ldots (9)$$

Thermal conductivity (Maxwell model):

$$\frac{k_{hnf}}{k_{bf}} = (C + 2k_{bf} + 2C - 2D) \times (C + 2k_{bf} - C + D)^{-1} \quad \ldots (10)$$

Where $= \frac{\varphi_{GO}k_{GO} + \varphi_{Ag}k_{cu}}{\varphi}$; $D = \varphi k_{bf}$

The specified dimensionless variables as detailed below:

$$X = \frac{x}{L};\ Y = \frac{y}{L};\ t = \frac{t^* U_0}{L};\ U = \frac{u}{U_0};\ V = \frac{v}{U_0};\ P = \frac{p}{\rho_{hnf} U_0^2};\ \theta = \frac{T - T_c}{T_h - T_c} \quad \ldots (11)$$

The non-dimensionalized forms of the partial differential Eqs (PDEs) (1) through (4) are presented below:

$$\frac{\partial U}{\partial X} + \frac{\partial V}{\partial Y} = 0 \quad \ldots (12)$$

$$\frac{\partial U}{\partial t} + U\frac{\partial U}{\partial X} + V\frac{\partial U}{\partial Y} = -\frac{\partial P}{\partial X} + \left[\frac{\nu_{hnf}}{\nu_{bf}}\right]\frac{1}{Re}\left[\frac{\partial^2 U}{\partial X^2} + \frac{\partial^2 U}{\partial Y^2}\right] \quad \ldots (13)$$

$$\frac{\partial V}{\partial t} + U\frac{\partial V}{\partial X} + V\frac{\partial V}{\partial Y} = -\frac{\partial P}{\partial Y} + \left[\frac{\nu_{hnf}}{\nu_{bf}}\right]\frac{1}{Re}\left[\frac{\partial^2 V}{\partial X^2} + \frac{\partial^2 V}{\partial Y^2}\right] - \left[\frac{\rho_{bf}}{\rho_{hnf}}\right]\left[\frac{\sigma_{hnf}}{\sigma_{bf}}\right]\frac{Ha^2}{Re}V + \frac{(\rho\beta)_{hnf}}{\rho_{hnf}\beta_{bf}}Ri\theta \quad \ldots (14)$$

$$\frac{\partial \theta}{\partial t} + U\frac{\partial \theta}{\partial X} + V\frac{\partial \theta}{\partial Y} = \frac{\alpha_{hnf}}{\alpha_{bf}}\frac{1}{Pr\,Re}\left[\frac{\partial^2 \theta}{\partial X^2} + \frac{\partial^2 \theta}{\partial Y^2}\right] + \left[\frac{\alpha_{hnf}}{\alpha_{bf}}\right]\frac{1}{RePr}Q\theta \quad \ldots (15)$$

Nusselt number for average and Local

$$Nu_{avg} = \int_0^1 Nu\, dX \quad \text{and} \quad Nu = -\frac{k_{hnf}}{k_{bf}}\left(\frac{\partial \theta}{\partial Y}\right)_{Y=0} \quad \ldots (16)$$

Numerical Procedure

MAC Formulation

The specified governing equations are solved using a finite difference scheme with forward and backward differencing for the non-dimensional system, where second derivatives are evaluated via quotient approximations. The discretized equations are analyzed using the Marker-and-Cell (MAC) method, as detailed in Refs. [23–25], with the algorithm flow as outlined in Fig. 2. The domain is divided into cells of size Δx and Δy, with velocity components defined at cell-face centers and pressure and temperature at cell centers. Cells are indexed as (i, j), where $p_{i,j}$denotes the cell-center pressure and $u_{i,j}$the x-velocity at the vertical face between open(i, j) and $(i+1, j)$,

The following equation represents the final form of the X-momentum equation used to determine the X-momentum at the next time step.

$$U^{n+1} = U^n - dt\left[U\frac{\partial U}{\partial X} + V\frac{\partial U}{\partial Y}\right] + \alpha_1\left[\frac{\partial^2 U}{\partial X^2} + \frac{\partial^2 U}{\partial Y^2}\right]dt \quad \ldots (17)$$

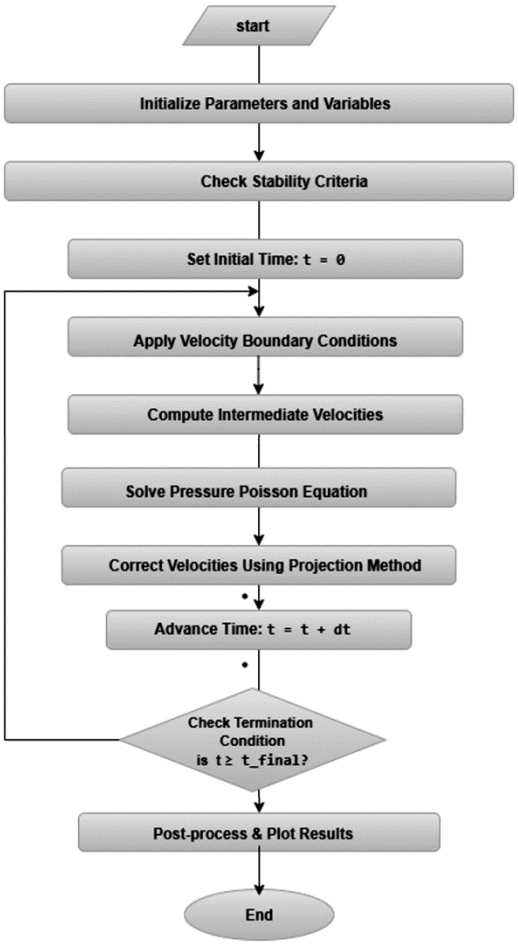

Fig. 2 — MAC algorithm

The final velocity equation in Y direction for the next time step, V^{n+1} a discretization method is employed.

$$V^{n+1} = V^n - dt\left[U\frac{\partial V}{\partial X} + V\frac{\partial V}{\partial Y}\right] + \alpha_1\left[\frac{\partial^2 V}{\partial X^2} + \frac{\partial^2 V}{\partial Y^2}\right]dt - \alpha_2 \mathrm{V}dt + \alpha_3 Ri\theta dt \quad \ldots (18)$$

The final energy equation, discretized for the next time step, (θ^{n+1}) is obtained in the following manner:

$$\theta^{n+1} = \theta^n - dt\left[U\frac{\partial V}{\partial X} + V\frac{\partial V}{\partial Y}\right] + \alpha_4\left[\frac{\partial^2 \theta}{\partial X^2} + \frac{\partial^2 \theta}{\partial Y^2}\right]dt + \alpha_4 Q\theta dt \quad \ldots (19)$$

where, $\alpha_1 = \frac{1}{Re}$, $\alpha_2 = \frac{Ha^2}{Re}$, $\alpha_3 = \frac{(\rho\beta)_{hnf}}{\rho_{hnf}\beta_{bf}}$, $\alpha_4 = \frac{1}{Pr\,Re}$

Table 2 — Grid-independent Test for Average Nusselt Number (Nu_{Avg})

Grid size	Nu_{Avg}
40×40	1.4373
50×50	3.0388
80×80	4.0190
100×100	4.3735

Grid independence study

Table 2 presents the variation of the maximum and mean Nusselt numbers, as well as the stream function extrema, with increasing grid resolution. The grid independence study confirmed that a 100×100 mesh provides sufficient accuracy for the present analysis. The simulations are performed for P r= 6.2, Q = 1, Re = 10, Ri = 1, and Ha = 10.

Results and Discussion

Fig. 3 exhibits periodic vortex formation and oscillatory scalar transport of Reynolds number. At early times, symmetric primary vortices emerge from wall shear layers, with rotation intensity increasing with Re. As time progresses, vortices undergo stretching and slight phase shifts, indicating inertial effects dominating over viscous damping at higher Re. Temperature contours evolve from smooth, diffusion-dominated profiles (Re = 1) to strongly advected structures (Re ≥ 2) with alternating thermal plume penetration. The X-shaped hot/cold intrusions result from periodic vortex sweeping, intensifying thermal mixing. Time histories of domain-averaged Nusselt number show low-amplitude oscillations for Re = 1, transitioning to higher-frequency, larger-amplitude fluctuations for Re = 3. This reflects the shift from quasi-steady conduction–convection balance to vortex-driven pulsating convection. Physically, the unsteady nature enhances mixing and transient heat transfer but also produces localized heat-flux peaks, which may be critical for thermal management in confined geometries. High-*Re* cases achieve better global transport yet risk larger instantaneous temperature gradients.

The streamline and isotherm patterns depicted in Fig. 4 clearly demonstrate the transition in flow and thermal characteristics with varying Richardson number. At a low value of *Ri*=0.1, the streamlines exhibit two nearly symmetric counter-rotating vortices, indicating that the flow is dominated by inertial forces with negligible buoyancy influence. In this regime, the isotherms remain largely horizontal and parallel to the heated and cooled sections,

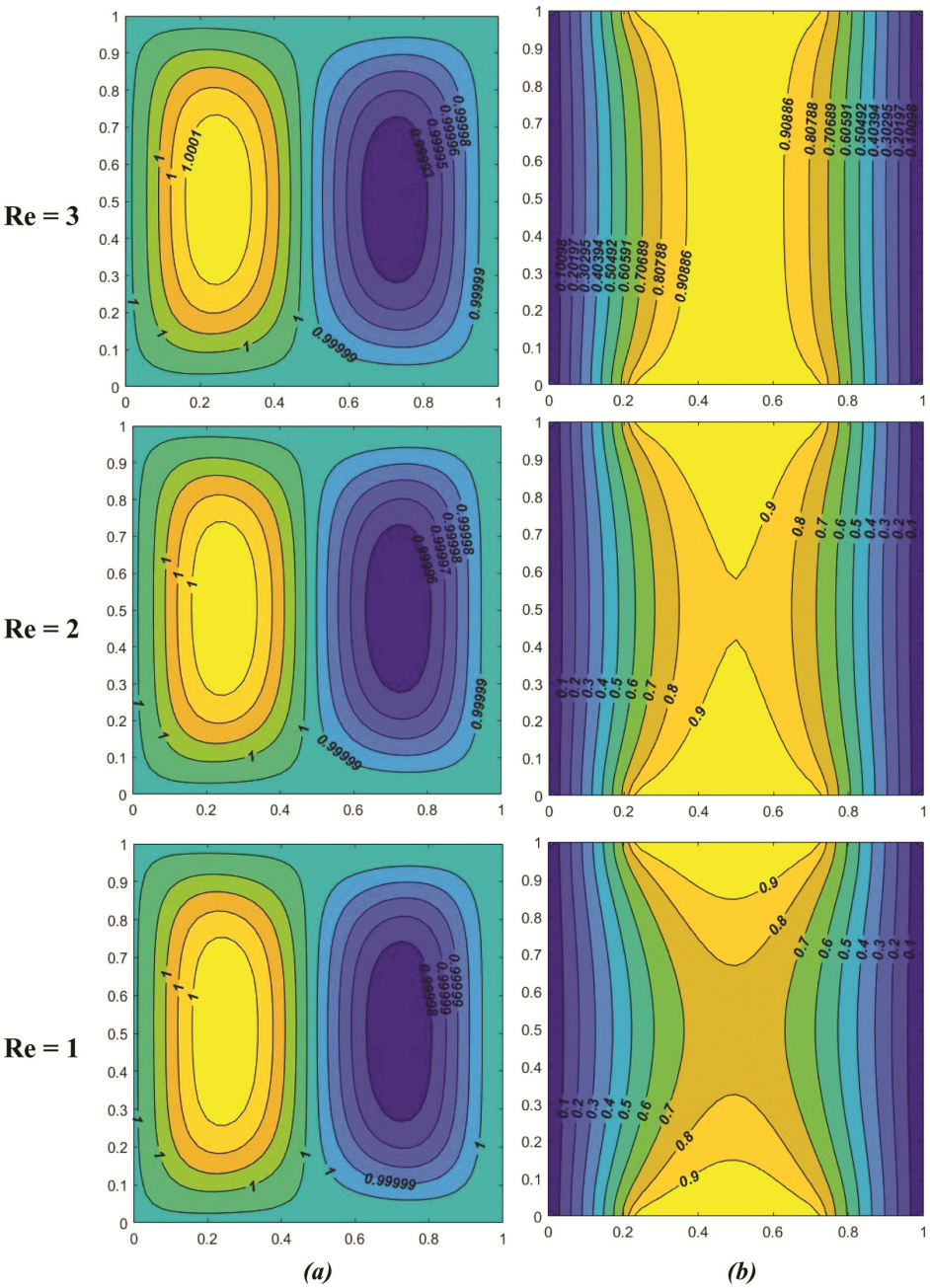

Fig. 3 — Streamlines (a) and isotherms (b) $Q = 6, Ri = 0.1, Pr = 6.2, Ha = 10$

suggesting that advection is the primary heat transport mechanism and thermal stratification is minimal. When Ri increases to 1, the streamlines become slightly elongated in the vertical direction, reflecting the comparable influence of buoyancy and inertia. This change is accompanied by a noticeable bending of isotherms toward the vertical walls, signifying stronger coupling between the velocity and temperature fields. At a higher value of *Ri*=10, buoyancy forces become dominant, causing the streamlines to shift upward with asymmetric circulation cells concentrated toward the top of the enclosure. Correspondingly, the isotherms display pronounced vertical clustering near the heated and cooled boundaries, indicating intensified thermal stratification and reduced horizontal mixing. These observations confirm that the Richardson number significantly governs the relative dominance of forced

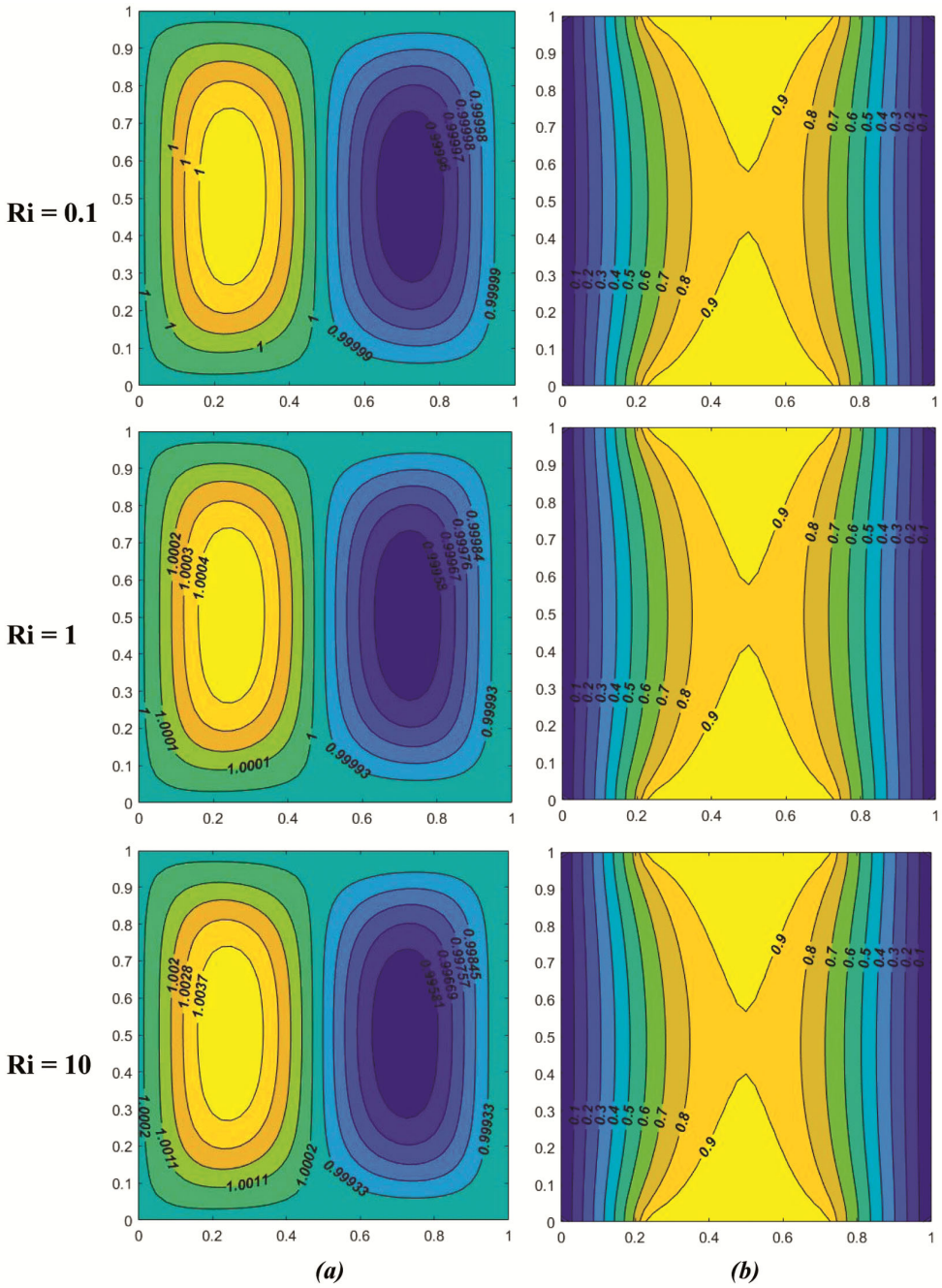

Fig. 4 — Streamlines (a) and isotherms (b) $Q = 6, Re = 2, Pr = 6.2, Ha = 10$

and natural convection modes, thereby altering both the flow topology and the thermal distribution within the cavity. A comparison of the computed Average Nusselt Number with Richardson number with reference to published literature is given in Table 3.

The streamline and isotherm distributions in Fig. 5 illustrate the influence of the internal heat generation parameter Q on the flow and temperature fields within the enclosure. For the case without heat generation

Table 3 — Comparison of the computed Average Nusselt Number (Nu_{Avg}) with Richardson number

(Ri)	Iwatsu *et al.*[26]	Oztop *et al.*[27]	Present
1.0	1.34	1.30	1.32
0.06	3.62	3.63	3.66
0.01	6.29	6.34	6.39

(Q=0), the streamlines reveal two symmetric counter-rotating vortices, indicative of a balanced forced convection regime. The isotherms are moderately

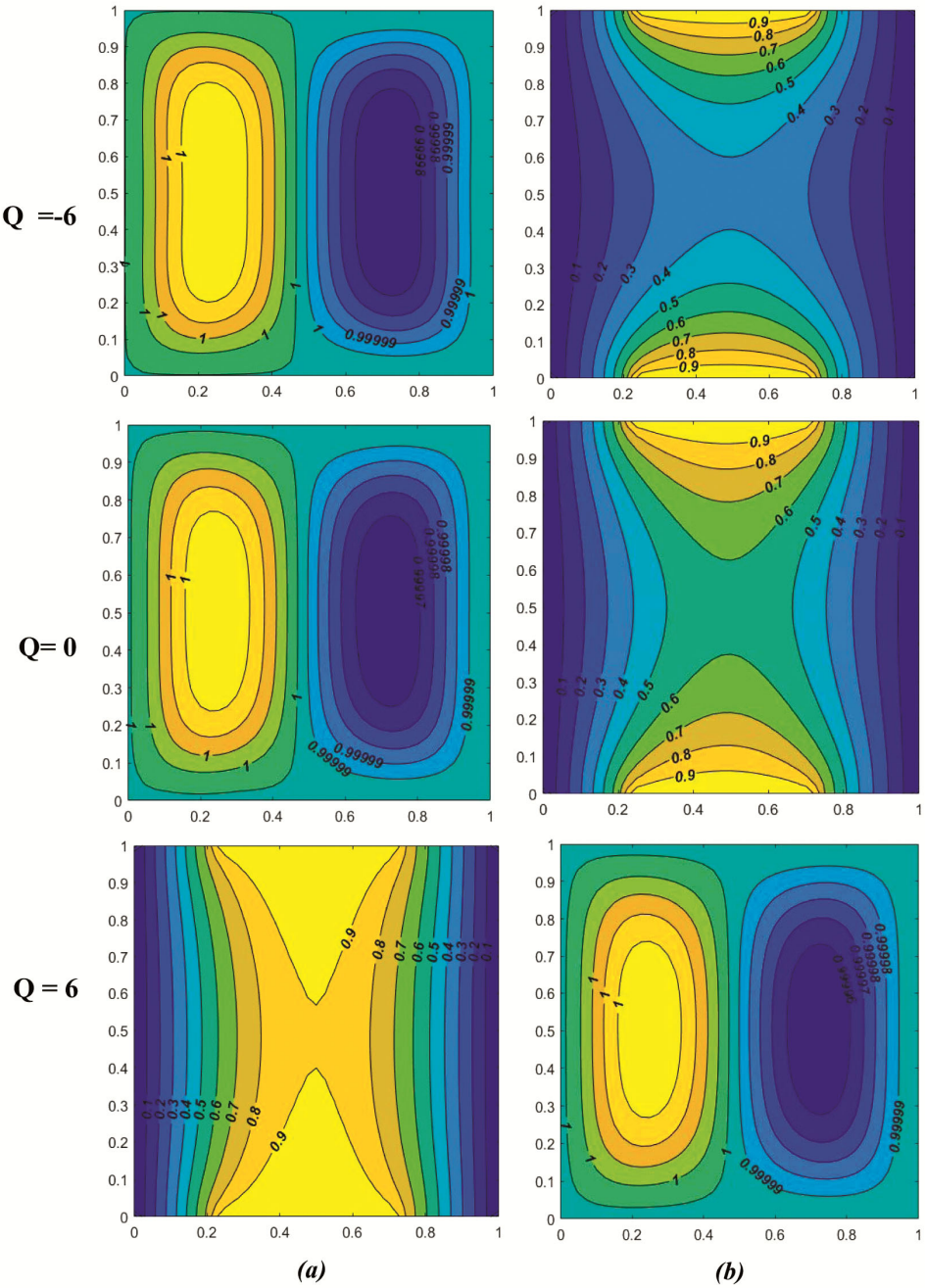

Fig. 5 — (a) Streamlines and (b) isotherms at $Ri = 0.1$, $Re = 2, Pr = 6.2, Ha = 10$

distorted near the heated and cooled regions but remain relatively smooth, suggesting that heat transfer is primarily driven by advection with limited thermal accumulation in the core region. When Q is increased to 6, the streamlines maintain their general twin-vortex structure but exhibit a slight contraction of the core region due to the buoyancy enhancement from internal heat generation. The isotherms, however, display a marked change: temperature contours become more closely spaced near the heated zone, and thermal gradients intensify, particularly along the upper portions of the cavity. This behavior reflects increased thermal energy storage within the fluid and stronger vertical stratification. The right-hand plots for Q=6 further emphasize that heat generation leads to higher temperature levels in the enclosure, compressing isotherms near cold boundaries and altering the thermal boundary layer thickness. These

results confirm that internal heat generation significantly modifies the thermal field while only slightly altering the overall flow topology.

Conclusion

The present study elucidates the coupled influence of buoyancy, inertia, and internal heat generation on forced convection of a Cu–GO/water hybrid nanofluid within a square enclosure. Variations in the Richardson number (*Ri*) govern the dominant transport mechanism, transitioning the system from inertia-driven symmetric vortices with weak thermal stratification at low *Ri* to buoyancy-controlled asymmetric circulations with pronounced vertical temperature layering at high *Ri*. Internal heat generation (Q) acts as an additional buoyancy source, elevating the fluid temperature, steepening local gradients, compressing isotherms near cold boundaries, and thinning the thermal boundary layer, while largely preserving the overall flow topology. The incorporation of Cu–GO nanoparticles significantly enhances the effective thermal conductivity and heat transfer capability of the water base fluid, enabling faster thermal equalization, reduced hot-spot formation, and improved control over thermal gradients compared to conventional single-particle nanofluids or pure water. This synergistic improvement makes the hybrid nanofluid particularly advantageous in real-time applications such as cooling of high-power-density electronic systems, thermal regulation in spacecraft modules, advanced solar thermal collectors, and efficient heat management in nuclear reactor cavities, where precise modulation of forced convection and enhanced heat removal are critical for performance and safety.

Conflict of Interest

The author declares no conflict of interest involved in this work.

Nomenclature

Symbol	Description
Pr	Prandtlnumber
G (ms^{-1})	gravitational acceleration
Nu	Local Nusselt number
Re	Reynolds number
P (pa)	pressure
Ri	Richardson number
T (K)	temperature
X	Dimensionless x-axis
Y	Dimensionless y-axis
U	Dimensionless velocity component in horizontal direction
V	Dimensionless velocity component in vertical-direction
X (m)	Cartesian coordinate in horizontal direction
Y (m)	Cartesian coordinate pin vertical direction
u (ms^{-1})	Dimensional velocity component in x-direction
v (ms^{-1})	Dimensional velocity component in y-direction
Q(Ws^{-2})	Heat flux
T_h (K)	Temperature of Hot wall
T_c (K)	Temperature of Cold wall
Ha	Hartmann number
B_0 (T)	Magnetic flux intensity
L (m)	Horizontallengthofenclosure
Greek Letters	
α ($m^2 s^{-1}$)	Thermal diffusivity
θ	Dimensionless temperature
σ ($S\ m^{-1}$)	Electric conductivity
β (K^{-1})	Coefficient of thermal expansion
μ ($kg\ m^{-1}\ s^{-1}$)	Dynamic viscosity value
ρ_{hnf} ($kg\ m^{-3}$)	Hybrid Nanofluid Density value
Subscripts	
c	Cold state value
h	Hot state value
bf	Base fluid state value
nf	Nanofluid value
hnf	Hybrid nanofluid value

Reference

1 Yang Y, Pu W, Yao Z, Zhang Q, Wang J & Han D, Experimental and numerical investigations on the intermittent heat transfer performance of rectangular cavity plate fin phase change material based heat sink, *J Energy Storage*, 60 (2023) 106607.

2 Alsabery A I, Gedik E, Chamkha A J & Hashim I, Effects of two-phase nanofluid model and localized heat source/sink on natural convection in a square cavity with a solid circular cylinder, *Comput Methods Appl Mech Eng*, 346 (2019) 952.

3 Armaghani T, Sadeghi M S, Rashad A M, Mansour M A, Chamkha A J, Dogonchi A S & Nabwey H A, MHD mixed convection of localized heat source/sink in an Al_2O_3-Cu/water hybrid nanofluid in L-shaped cavity, *Alex Engi J*, 60 (2021) 2947.

4 Waqas H, Hasan M J, Majeed A H, Liu D & Muhammad T, Hydrothermal characteristics, entropy and kinetic energy investigation in a sinusoidal cavity for variable wavelengths

and solid volume fraction using Cu-water nanofluid, *J Mol Liq*, 389 (2023) 122911.
5 Asmadi M S, Kasmani R M, Siri Z & H Saleh, Novel enhanced thermal capabilities of Cu-Al2O3/water hybrid nanofluid in an oblique U-shape cavity: On the molecular behaviour through vorticity analysis, *J Mol Liq*, 400 (2024) 124545.
6 Rajarathinam M, Akermi M, Khan M I & Nithyadevi N, MHD mixed convection heat transfer of copper water nanofluid in an inclined porous cavity having isothermal solid block, *J Magn Magn Mater*, 593 (2024) 171845.
7 Rashad A M, Armaghani T, Chamkhaand A J & Mansoure M A, Entropy generation and HD natural convection of a nanofluid in an inclined square porous cavity: Effects of a heat sink and source size and location, *Chin J Phys*, 56 (2018) 193.
8 Moayedi H, Investigation of heat transfer enhancement of Cu-water nanofluid by different configurations of double rotating cylinders in a vented cavity with different inlet and outlet ports, *Int Commun Heat Mass Transf*, 126 (2021) 105432.
9 Emami R Y, Siavashi M & Moghaddam G S, The effect of inclination angle and hot wall configuration on Cu-water nanofluid natural convection inside a porous square cavity, *Adv Powder Technol*, 29 (2018) 519.
10 Ebrahimi A & Dadvand A, Simulation of melting of a nano-enhanced phase change material (NePCM) in a square cavity with two heat source–sink pairs change material (NePCM) in a square cavity, *Alex Eng J*, 54 (2015) 1003.
11 Rashad A M, Ismael M A, Chamkha A J & Mansour M A, MHD mixed convection of localized heat source/sink in a nanofluid-filled lid-driven square cavity with partial slip, *J Taiwan Inst Chem Eng*, 68 (2016) 173.
12 Faraz N, Nisar M S, Khan Y, Hussain A & Iqbal K, Natural convection of Cu-H_2O nanofluid inside hexagonal enclosure fitted with a square cavity with a non-uniformly heated walls, *Results Phys*, 51 (2023) 106648.
13 Hidki R, Moutaouakil L E, Boukendil M, Charqui Z, Zrikem Z & Abdelbaki A, Impact of Cu, Al_2O_3-water hybrid nanofluid on natural convection inside a square cavity with two heat-generating bodies, *Mater Today: Proc*, 72 (2023) 3749.
14 Vinodhini N & Prasad V R, Simulation of natural convection in a square cavity with micropolar fluid and magnetic fields using FVM, *Indian J Chem Technol*, 31 (2024) 902.
15 Baithalu R & Mishra S R, Sensitivity analysis of various factors on the micropolar hybrid nanofluid flow with optimized heat transfer rate using response surface methodology: A statistical approach, *Phys Fluids,* 35 (2023) 102016.
16 Iqbal Z, Ali F, Xu H, Zhu X, Alqarni M M, Hussain A, Alhazmi S E, Ragab E M & Ahmed M F, Numerical simulations of thermal convection in unsteady darcy forchheimer flow of radiative hybrid nanofluid over a slipping spinning porous disk, *Case Stud Therm Eng*, 68 (2025) 105826
17 Reddy M V, Nath J M, Ali F, Das T K, Khan U & Garayev M, Implementation of homotopy analysis method for entropy-optimized two-phase nanofluid flow in a bioconvective non-Newtonian model with thermal radiation, *J Radiat Res Appl Sci*, 18 (2025) 101218.
18 Prakash R, Kamatchi R & Devanathan R S, Turbulent natural convection heat transfer enhancement of Nanofluids, *J Phys*, 2484 (2023) 012035.
19 Mansour M A, Siddiq S, Gorla R S R & Rashadd A M, Effects of heat source and sink on entropy generation and MHD natural convection of Al_2O_3-Cu/water hybrid nanofluid filled with square porous cavity, *Therm Sci Eng Prog*, 6 (2018) 57.
20 Algehyne E A, Alharbi A F, Saeed A, Dawar A, Ramzan M & Kumam P, Analysis of the MHD partially ionized GO-Ag/water and GO-Ag/kerosene oil hybrid nanofluids flow over a stretching surface with Cattaneo-Christov double diffusion model: A comparative study, *Int Commun Heat Mass Transf*, 136 (2022) 106205.
21 Ahmad F, Abdal S, Ayed H, Hussain S, Salim S & Almatroud A O, The improved thermal efficiency of Maxwell hybrid nanofluid comprising of graphene oxide plus silver/kerosene oil over stretching sheet, *Case Stud Therm Eng*, 27 (2021) 101257.
22 Ghadikolaei S S & Gholinia M, 3D mixed convection MHD flow of GO-MoS_2 hybrid nanoparticles in H_2O-$(CH_2OH)_2$ hybrid base fluid under the effect of H_2 bond, *Int Commun Heat Mass Transf*, 110 (2020) 104371.
23 Vinodhini N & Prasad V R, Numerical study of magneto convective Buongiorno nanofluid flow in a rectangular enclosure under oblique magnetic field with heat generation/absorption and complex wall conditions, *Heliyon*, 9 (2023) e17669.
24 Vinodhini N & Prasad V R, Numerical study of free convection ag-water nanofluid flow in a square enclosure with viscous dissipation and heat generation/absorption effects in a porous medium with complex wall conditions, *J Porous Media*, 26 (2023) 77.
25 Vinodhini N & Prasad V R, Magneto-hybrid nanofluid (Al_2O_3/Cu-Oil) flow in a porous square enclosure with Cattaneo-Christov heat flow model-sensitivity analysis, *Indian J Chem Technol*, 30 (2023) 714.
26 Iwatsu R, Hyun J M & Kuwahara K, Mixed convection in a driven cavity with astable vertical temperature gradient, *Int J Heat Mass Transf*, 36 (1993) 1601.
27 Oztop H F, Zhao Z & Yu B, Fluid flow due to combined convection in lid driven enclosure having circular body, *Int J Heat Fluid Flow*, 30 (2009) 886.